International Journal of Micro Air Vehicles

Article

International Journal of Micro Air Vehicles
2017, Vol. 9(3) 218–231

DOI: 10.1177/1756829317702048
journals.sagepub.com/home/mav
SAGE

# Development of a meso-scale cycloidal-rotor aircraft for micro air vehicle application

**Elena Shrestha[1], Derrick Yeo[1], Moble Benedict[2] and Inderjit Chopra[1]**

## Abstract

This paper describes the design, controls system development, and hover testing of a 60-g meso-scale cycloidal-rotor based (cyclocopter) micro air vehicle. The cycloidal rotor (cyclorotor) is a revolutionary vertical take-off and landing concept with a horizontal axis of rotation. The twin-cyclocopter utilizes two optimized cyclorotors and a horizontal tail rotor used to counteract the pitching moment generated by the cyclorotors. An innovative light-weight and high strength-to-weight ratio blade design significantly reduced cyclorotor weight and improved aerodynamic efficiency. In addition, increasing the virtual camber and incidence (by increasing chord-to-radius ratio) and using a symmetric pitching schedule with a maximum $\pm 45^{\circ}$ pitching amplitude also improved rotor efficiency. Due to gyroscopic coupling and inherent instability of the cyclocopter, a closed-loop feedback control system was implemented using a custom autopilot weighing 1.5 g. The 60-g meso-scale twin-cyclocopter successfully demonstrated stable, sustained hover.

## Keywords

Cyclocopter, cyclogyro, cyclorotor, cycloidal rotor, Micro air vehicle, MAV, meso-scale

Date received: 20 May 2015; accepted: 21 March 2016

## Introduction

Recently, there has been widespread interest in developing a robust and versatile, palm-sized micro air vehicle (MAV) platform for both commercial and military scenarios. MAVs were formally defined as aircraft with maximum dimension of 15 cm and maximum weight of 100 g by the Defense Advanced Research Projects Agency (DARPA) in 1997.[1] Meso-scale UAVs are between DARPA's definition of nano-scale (<20 g) and micro-scale (<100 g) in terms of weight and vehicle dimension. DARPA intended to develop MAVs for military missions such as reconnaissance, search-and-rescue, and border surveillance. In the last decade, there has been an increase of commercial interest in MAVs capable of precision package delivery, aerial photography, and even traffic monitoring. These wide varieties of applications require an MAV platform with high endurance, maneuverability, gust tolerance, and hover/high-speed flight capability. In the past, rotary-winged MAV configurations such as single main rotor (SMR), co-axial, and compound have been developed to fulfill these requirements. For commercial applications, many companies have been relying on multi-rotor configurations with fixed pitch setting and controls through rotor r/min variation. While successful at larger scales, conventional edgewise rotors have degraded performance at low Reynolds number (10,000–50,000) at which meso-scale UAVs operate.[2,3]

[1]Department of Aerospace Engineering, Alfred Gessow Rotorcraft Center, University of Maryland, College Park, MD, USA
[2]Department of Aerospace Engineering Texas A&M University College Station, TX, USA

**Corresponding author:**
Elena Shrestha, Department of Aerospace Engineering, Alfred Gessow Rotorcraft Center, University of Maryland, College Park 20742, MD, USA.
Email: eshresco@gmail.com

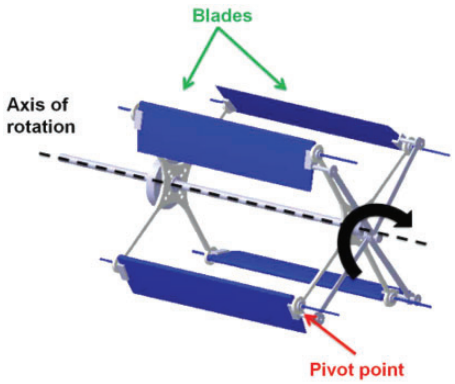


**Figure 1.** Cycloidal rotor.

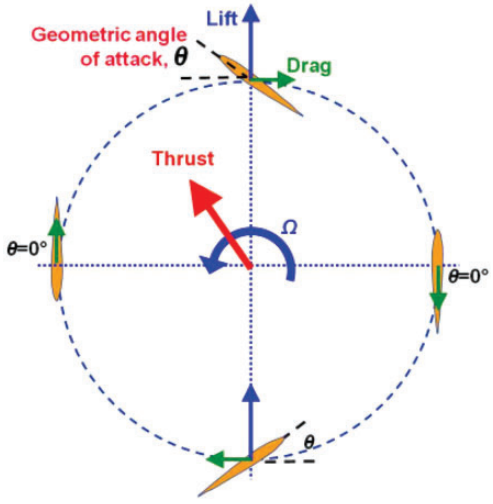


**Figure 2.** Blade kinematics.

An efficient alternative to conventional edgewise rotor is the cycloidal rotor (cyclorotor), a horizontal axis propulsion system where the blades follow a circular trajectory about a horizontal axis of rotation (Figure 1). The cyclorotor blade span is parallel to the axis of rotation and perpendicular to the direction of flight. A pitching mechanism cyclically varies individual blade pitch angle along a circular trajectory. In hover, the blades achieve a positive geometric pitch angle at both the top and bottom portions of the trajectory, yielding a net resultant thrust in one complete revolution (Figure 2). Both the magnitude and direction of the thrust vector can be adjusted by varying the pitch amplitude and phasing of the blade pitching kinematics.

When compared to a conventional edgewise rotor at the same disk loading (thrust/disk area), an optimized cyclorotor has a higher power loading (thrust/power) in hover (Figure 3). Since all spanwise blade sections of the cyclorotor operate under similar aerodynamic

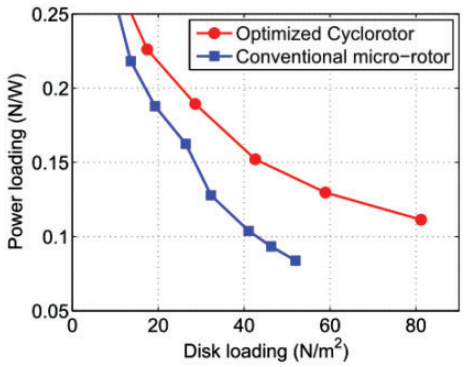


**Figure 3.** Power loading (thrust/power) vs. disk loading for conventional micro-rotors and optimized cyclorotor.

conditions, the blades can be optimized to achieve best aerodynamic efficiency. In addition, the uniform spanwise distribution of aerodynamic forces enables the cyclorotor to operate at lower tip speeds, thereby improving the acoustics signature. Previous PIV studies have also shown existence of beneficial unsteady aerodynamic mechanisms, such as leading edge vortices that delay the onset of blade stall and improve the lift producing capability and aerodynamic efficiency of the cyclorotor.[4–6]

Another advantage of the cyclorotor is its unique thrust vectoring capability that is achieved by varying the phase of the cyclic pitching. By thrust vectoring instead of pitching forward, the cyclocopter can achieve level forward flight in a power-efficient manner. Previous wind tunnel studies on an isolated cyclorotor found that thrust vectoring enables a cyclocopter to potentially reach up to 13 m/s (29 mph) without relying on additional lift augmenting devices/surfaces.[7] It was observed that the power required for a cyclorotor to maintain a steady, level flight significantly drops with forward speed (Figure 4), up to almost an advance ratio of 1.0, due to increased lift producing efficiency of the cyclorotors. Thrust vectoring also improves maneuverability and capability of operating in gusty environments.

Since 2011, the University of Maryland has successfully developed a series of hover and forward flight-capable cyclocopters ranging from 130 to 800 g.[9–12] Previously, cyclocopters less than 100 g were not feasible because of the high empty weight fraction penalty and aerodynamic inefficiency from cyclorotors at the meso-scale ($Re < 20{,}000$). Developing a highly compact and portable cyclocopter would aid in both military and commercial applications such as surveillance and search-and-rescue. Reducing the vehicle's footprint enables operation in highly constrained environments, reduces visual detection and acoustics, and eases portability. Therefore, the present research focuses on developing a hover-capable 60 g meso-scale

twin-cyclocopter with significant improvements in blade design and controls system to account for gyroscopic coupling. The 60-g vehicle developed in this research is the lightest cyclocopter in literature to have flown successfully (Figure 5).

In addition to vehicle development, this paper will provide a weight breakdown and rotor performance comparison of twin-cyclocopters at various scales (60 g, 130 g, 235 g, and 550 g) to identify key parameters dictating vehicle weight and performance. One of the biggest challenges is that many of the electronics and motors are limited by commercial availability. In addition, the maximum efficiency of motors decreases with size.[13] Another challenge is because of lower inertia and faster vehicle dynamics compared to cyclocopters at larger scales, the autopilot requires a higher processing rate in order to stabilize the vehicle. This paper will first outline vehicle development and then present a detailed overview of blade design, rotor performance, controls system with custom autopilot, and the gyroscopic decoupling method. Finally, flight testing results will show a stable, sustained hover along with attitude data from the onboard processor.

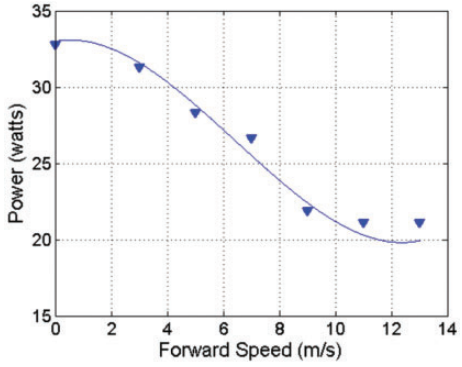


**Figure 4.** Power versus forward speed for constant rotational speed of 1740 r/min (13.88 m/s) for level, steady flight.

## Vehicle development

One of the key factors in developing a meso-scale cyclocopter is reducing the vehicle's high empty weight fraction. Because majority of the weight is from the cyclorotors with each rotor utilizing four composite blades, the main focus was on designing lightweight blades with high bending and torsional stiffness. The developed 60 g twin-cyclocopter utilizes two cyclorotors and a horizontal tail rotor to counterbalance the pitching reaction moment from the cyclorotors rotating in the same direction. Anti-torque capability from the tail rotor is also augmented by increasing the horizontal offset between the rotor and vehicle's center of gravity (c.g.). The offset reduces the thrust required from the tail rotor and minimizes the rotor size.

An important criterion for MAVs in both military and commercial application is compactness. As explained before, reducing the vehicle's footprint enables operation in highly space-confined environments. Therefore, the present cyclocopter has a minimal lateral dimension of 0.178 m (7 inches), longitudinal dimension of 0.127 m (5 inches), and a height of 0.152 m (6 inches). Each cyclorotor has a diameter of 0.076 m (3 inches), blade span of 0.043 m (1.70 inches), a chord of 0.022 m (0.85 inches), and uses a NACA 0015 airfoil. The blades on the cyclorotors achieve symmetric pitching with maximum pitching amplitude of 45°. These parameters (blade pitching amplitude, location of pitch axis, rotor radius, blade airfoil, chord, planform, etc.) of the present cyclorotor have been optimized based on previous parametric studies[14–18] and additional experimental studies performed in this research that will be discussed in the following sections. Leveraging the insights gained from these

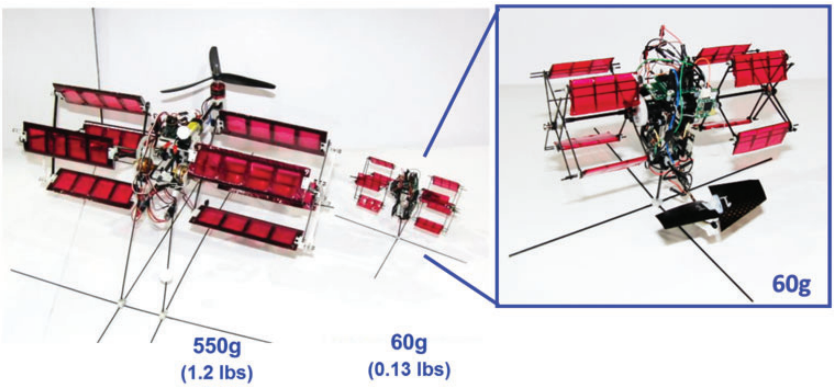


**Figure 5.** 60 gram meso-cyclocopter compared to a 550 g cyclocopter.

studies, the present cyclorotor is designed for maximum thrust-to-power ratio (power loading) in hover.

Both the motor and gear ratios were selected through a parametric test minimizing electrical power (W). While the 4.2 g ADC5 motor drew the least amount of power at the operating cyclorotor thrust level, the 3.6 g increase in weight from the three rotors (compared to using the lighter AP-03 (3 g)) would nullify any performance advantage (Figure 6). From the three different gear ratios that were tested (6:1, 7:1, and 7.5:1), the 7:1 ratio provided the best electrical power efficiency for the AP-03 motor (Figure 7). Therefore, each rotor is independently driven by an AP-03 4000KV brushless outrunner motor and the cyclorotors are connected to a 7:1 single-stage transmission while the tail rotor is directly driven by the brushless motor.

The motors are controlled by the onboard avionics through a YEP 7 A electronic speed controller (ESC) weighing 1.5 g. All three rotors are powered by a single 2 S 7.6 V 250 mAh Lithium-Polymer (LiPo) battery.

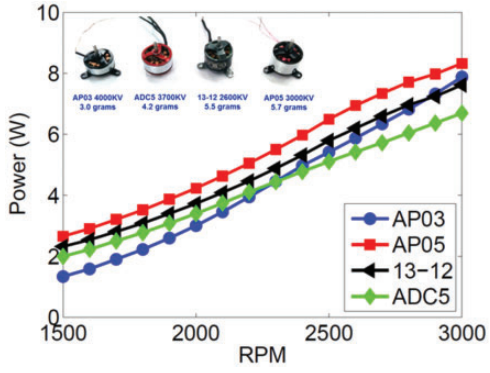


**Figure 6.** Electrical power (W) curves at different r/min for the tested motors (7:1 transmission).

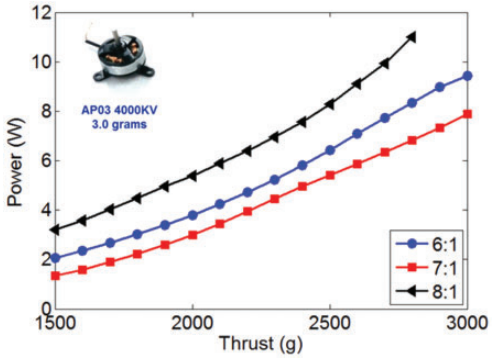


**Figure 7.** Electrical power (W) curves for AP-03 motor tested at different gear ratios.

The thrust vectoring mechanism on each cyclorotor is actuated by 1.8 g spectrum linear servos powered by a single cell 3.7 V 125 mAh LiPo battery. All of the actuators are controlled by a custom avionics board (autopilot) developed at the University of Maryland. The Embedded Lightweight Kinematic Autopilot (ELKA) board is one of the lightest autopilot developed for MAVs, weighing only 1.3 g. ELKA interfaces with a breakout board that connects to all the actuators and is powered by a dedicated single cell 3.7 V 125 mAh LiPo battery. A detailed weight distribution of all components is provided in Table 1.

Table 1 also summarizes the weight percent distribution of the previous twin-cyclocopters (130–550 g). From the weight distribution, it is evident that the cyclorotors make up the majority of the empty weight fraction of the vehicle. The cyclorotors consistently constitute 23–34% of the total gross weight and the range largely varies based on blade design. Therefore, significant effort was focused on designing lightweight and structurally robust blades and pitching mechanism in order to reduce total vehicle weight and increase endurance. Another noticeable trend is that the weight contribution of the transmission system (cyclorotor motors, gears, bearings, and associated screws) increases with vehicle scale.

As expected, the weight contribution from electronics (servos, ESCs, and associated wires) increases at smaller scales. That is because the size of the selected electronics is limited by what is commercially available. A similar trend is observed in the avionics (processor, breakout board, and satellite receiver) since all of these vehicles use the lightest available onboard processor. The LiPo batteries compose 14–19% of the total vehicle weight and are also limited by commercial availability. Overall, the most significant improvements to the vehicle design can be made through the cyclorotors, which directly affects the transmission system, anti-torque

**Table 1.** Weight distribution of previous generation twin-cyclocopters (60–550 g).

| System | 60 g (g) | 60 g (%) | 130 g (%) | 235 g (%) | 550 g (%) |
|---|---|---|---|---|---|
| Cyclorotors | 14 | 12 | 33 | 34 | 27 |
| Electronics | 10 | 16 | 17 | 14 | 11 |
| Propeller | 5 | 8 | 16 | 6 | 9 |
| Battery | 10 | 16 | 14 | 18 | 19 |
| Structure | 8 | 13 | 9 | 9 | 12 |
| Transmission | 7 | 12 | 7 | 17 | 21 |
| Avionics | 7 | 12 | 4 | 2 | 1 |

propeller size, and structural weight (landing gear, fuselage, etc.).

## Rotor performance

As seen from the weight distributions, the cyclorotors typically compose up to 25% of the vehicle's gross weight. To reduce the empty weight fraction, the cyclorotor blades must be carefully designed to be lightweight and structurally robust. The rotor structural design must be able to withstand the dominant centrifugal force because each gram of blade weight amounts to approximately 0.4 N of centrifugal load on the blade. In addition, the blades also need to have high strength-to-weight ratio to minimize the bending and torsional deformations caused by the transverse centrifugal loading.

For the 60 g cyclocopter, the initial blade had a monolithic design with a foam core wrapped in single ply of $\pm 45^{\circ}$ carbon fiber prepreg. The bending stiffness was provided by the thickness of the NACA 0015 airfoil and the torsional stiffness was from the carbon fiber orientation and the closed cross-sectional area. The pitching axis and linkage attachment point were on two separate delrin blade attachment pieces mounted on spanwise ends of the blade and contributed to the total blade weight (Figure 8). Besides the weight, a significant drawback of the design was inconsistent placement of the blade attachment pieces during the manufacturing process, which consequentially led to significant blade twist and decreased performance.

The new blade design (Figure 9) is a composite structure with a foam leading edge and carbon fiber ribs, spars, and stringers. The NACA 0015 ribs are milled out of carbon fiber and are evenly distributed along the span to maintain the airfoil shape. The pitching axis is provided by a carbon fiber spar that runs through the entire blade structure and an additional carbon fiber spar provides a connection to the blade pitch links. To prevent the Mylar from forming cavities between the ribs, multiple carbon fiber stringers are distributed chordwise along the blade. In addition, a single layer of foam outlines the leading edge to maintain a clearly defined airfoil shape. With the new design, bending and torsional stiffness is provided by the spars and stringers. The torsional stiffness is further augmented by the closed blade structure from the 50 micron thick mylar. The total weight of the new blade is 0.50 g compared to 1.50 g of the previous blade.

### *Blade design*

The cyclorotor performance can be attributed to four main design aspects: (1) blade structural design, (2) blade geometry, (3) rotor geometry, and (4) blade kinematics. Previous experimental parametric studies[12,17] showed that a key parameter in cyclorotor performance regarding blade and rotor geometry is the solidity ($\sigma$)

$$\sigma = \frac{N_b C}{2\pi R}$$

The solidity is affected by the number of blades ($N_b$) and chord-to-radius (c/R) ratio. On a conventional rotor, there is an optimum solidity that is directly influenced by the total blade area ($N_b cb$) at each thrust value. However, for the cyclorotor, changing the solidity by varying either ($N_b$) or c/R yields completely different results because of the different phenomenon involved. For a fixed c/R, changing the number of blades alters the total blade area and subsequently the solidity, which results in a similar effect on cyclorotor performance as on the conventional rotor. For a fixed number of blades, changing c/R not only affects the blade area, but also changes the flow curvature effect on the cyclorotor.[14]

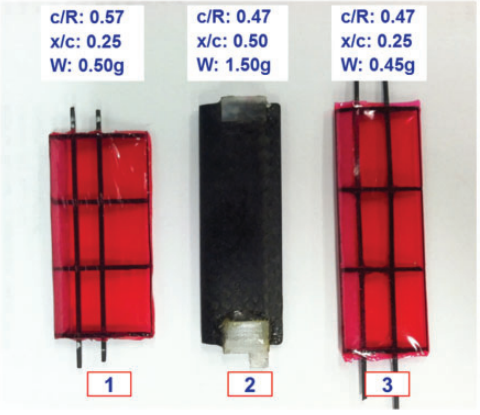


**Figure 8.** Different blades tested for the 60 g cyclocopter.

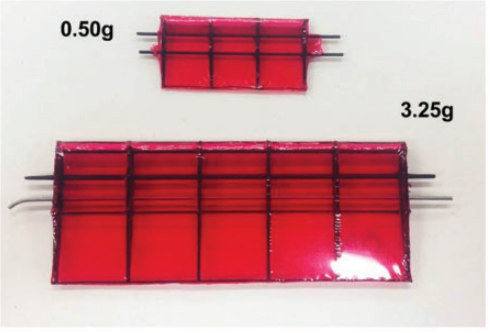


**Figure 9.** New blade design using rib and spar structures.

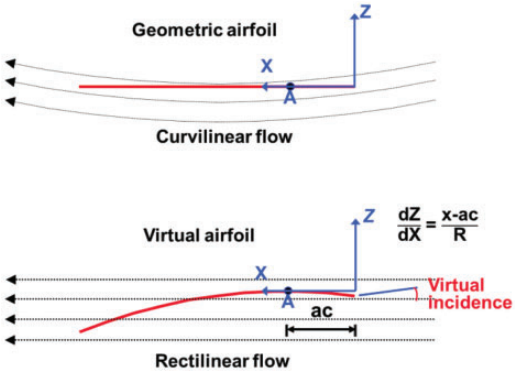


**Figure 10.** Virtual camber and incidence in a curvilinear flow.

The blades on the cyclorotor experience a virtual camber effect because of the curvilinear nature of the flow, which introduces a chordwise variation in velocity. Therefore, a symmetric airfoil at 0° pitch behaves as a virtually cambered airfoil at a virtual incidence (Figure 10) in a rectilinear flow. The blades experience a negative virtual camber and incidence at the top of the trajectory ($C_1 < 0$) and a positive camber and incidence at the bottom portion of the trajectory ($C_1 > 0$). The study found that virtual camber and incidence was proportional to the chord-to-radius ratio at higher values and location of the blade pitching axis. After systematically measuring the power loading (thrust/power) with disk loading (thrust/disk area) at various solidities and at 40° pitching amplitude, the maximum performance resulted from a four-bladed rotor with a c/R ratio of approximately 0.83. While aerodynamically efficient, the c/R of 0.83 would result in heavy blades with low aspect ratios (AR) and lead to increased structural loads on the blades. However, it should be noted that power loading did not drastically change when c/R was within 0.6 to 0.8.

The previous experiments were conducted on a larger cyclorotor with double the radius, operating at Reynolds number (Re) from 20,000 to 40,000. To determine if the results are accurate at the meso-scale (Re < 20,000), various blades were tested using Nano17, a commercial force-torque sensor (Figure 11). As seen in Figure 12, three different blades with the same planform area, but with variations in c/R ratio, blade geometry, and structure were tested for maximum power loading. Blade #2 uses the initial design and weighs 1.50 g with an aspect ratio of 2.86 (c = 0.70 in, b = 2.0 in) and c/R ratio of 0.47. To observe the effects of blade structure on performance, a newly designed blade (#3) with identical blade geometry and c/R was created and weighed approximately 0.45 g. The final 0.50 g blade (#1) has a lower AR of 2 (c = 0.85 in, b = 1.70 in) and a higher c/R of 0.57.

A linear approximation shows that the virtual chamber for blade #1 is approximately 7% of the blade

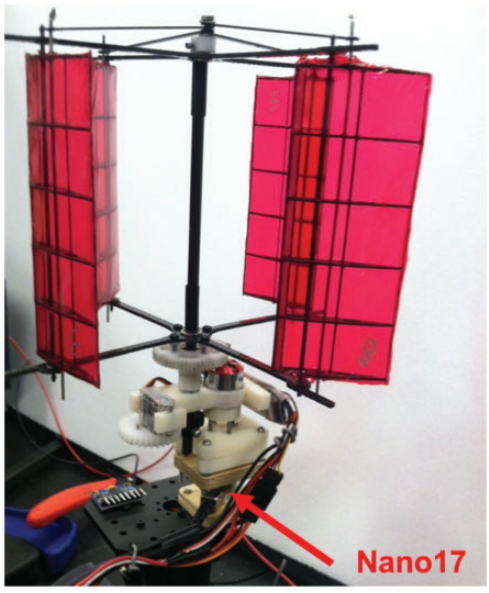


**Figure 11.** Force/torque sensor experimental setup.

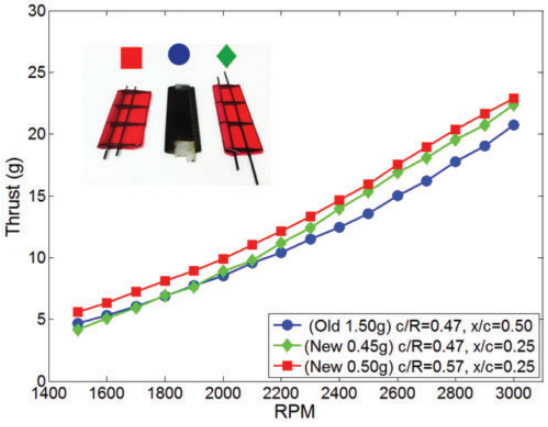


**Figure 12.** Thrust vs. r/min comparison of all blade designs.

chord while 5% of chord for blades #2 and #3.[19] Based on a similar linear model for virtual incidence, blade #1 experiences an 8° virtual incidence while blades #2 and #3 experience 6° of incidence. The pitching axis locations (x/c) of all blades were centered around the chordwise c.g. location, which resulted in x/c of 0.25 for the new blade designs and x/c of 0.50 for the old design. The pitching axis is aligned with the chordwise location of blade c.g. in order to reduce the pitching moments on the blade caused by the centrifugal force. In addition, it reduces the loads on the pitching mechanism and ultimately on the light-weight thrust vectoring linear servos with limited torque capacity (0.02 Nm). Table 2 provides a full summary of all the blade properties.

**Table 2.** Blade properties (60 g-scale cyclocopter).

| Parameter | Blade #1 | Blade #2 | Blade #3 |
|---|---|---|---|
| Weight (g) | 0.50 | 1.50 | 0.45 |
| Chord-to-radius (c/R) | 0.57 | 0.47 | 0.47 |
| Pitching axis (x/c) | 0.25 | 0.50 | 0.25 |
| Chord (in.) | 0.85 | 0.70 | 0.70 |
| Span (in.) | 1.70 | 2.00 | 2.00 |
| Virtual camber (%c) | 7.00 | 5.00 | 5.00 |
| Virtual incidence (°) | 8.00 | 6.00 | 6.00 |

%c: % of chord.

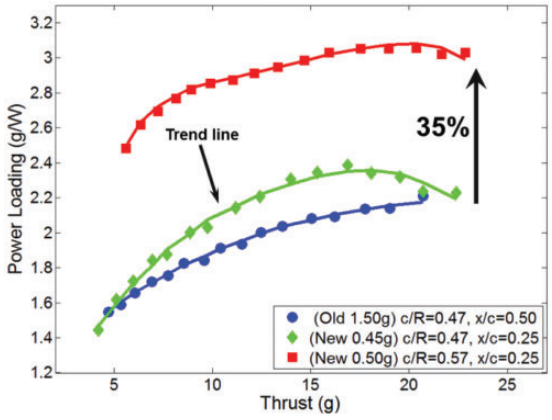


**Figure 13.** Electrical power loading vs. thrust shows 35% improvement of new blade design.

To determine the optimum blade design, both thrust and power loading were systematically measured for each blade from 1500 to 3000 r/min in increments of 100 r/min. When comparing the thrust, increased virtual chamber and incidence (blade #1) resulted in a higher thrust value at each r/min (Figure 12). Interestingly, even though blades #2 and #3 had the same blade geometry, the lighter 0.45 g blade (#3) produced more thrust at higher rotational speeds. One possibility for discrepancies in rotor performance could be that blade #3 experiences a lower centrifugal loading compared to the heavier 1.50 g blade since centrifugal force varies linearly with mass and square of blade velocity ($mV^2/R$). However, previous studies have shown that moving the pitching axis location closer to the leading edge steadily increases the thrust produced by the cyclorotor.[20] When comparing the power loading, the optimum pitching axis location should be between 35% and 45% of blade chord at higher disk loadings (thrust/disk area).

A comparison of power loading (thrust/electrical power) shows an increase of up to 35% of aerodynamic efficiency from blade #2 to blade #1 (Figure 13). The trend lines from these experiments agree with the previous studies on the effects of flow curvature on the cyclorotor. While increasing the c/R ratio appears to improve rotor efficiency, the overall blade geometry is also restricted by weight. There is a noticeable difference in efficiency between blades #2 and #3 caused by an increase in blade mass which proportionally leads to an increase in the centrifugal loading. However, the c/R ratio seems to have the most significant impact on cyclorotor performance.

Based on the results of the parametric study, the optimized cyclorotor on the 60 g twin-cyclocopter utilizes four 0.50 g blades with the new blade design, c/R ratio of 0.57, and pitching axis location at 25% of blade chord. Along with other structural components, the optimized cyclorotor weighs 7 g and has a thrust-to-weight (T/W) ratio of approximately 3 at the operating rotational speed of 3000 r/min (T = 23 g). This is a significant improvement to previous design iterations as evidenced by thrust and power loading trends.

## *Blade pitching mechanism*

Besides the blade structural design, blade geometry, and rotor geometry, blade kinematics plays an important role in cyclorotor performance. Previous experimental parametric studies varied pitching amplitudes and studied their effect on rotor performance.[20] For symmetric pitching, the 45° pitching amplitude achieved a higher maximum thrust at the tested rotational speeds. However, the optimum power loading was achieved with a 40° blade pitching amplitude followed by 45°. The reason for performance differences when comparing thrust and power loading is because power loading varies inversely with rotational speed. Therefore, it is more efficient to increase thrust by increasing blade pitching amplitude.

The maximum achievable blade pitching amplitude is limited by the onset of blade stall. Interestingly, flow field studies[4–6] suggested that the cyclorotor is able to increase thrust even at higher angles of attack (±45°) because of a pitch-rate induced stall delay on the blades. PIV measurements also suggested a distinct leading edge vortex and constructive blade vortex interactions which may be augmenting the lift-producing capabilities of the cyclorotor. Based on these results, the present meso-scale cyclorotor is designed with a 45° symmetric blade pitching.

The schematic of the blade pitching mechanism is depicted in Figure 14 where the four bars of the linkage system are labeled $L_1$, $L_2$, $L_3$, and $L_4$. The link $L_1$, also referred to as rotor radius, is the distance between the blade pitching axis and the horizontal axis of rotation. The pitch links ($L_3$) are connected to the end of the offset link on one end and the other end is connected to point B which is at a distance $L_4$ behind the pitching

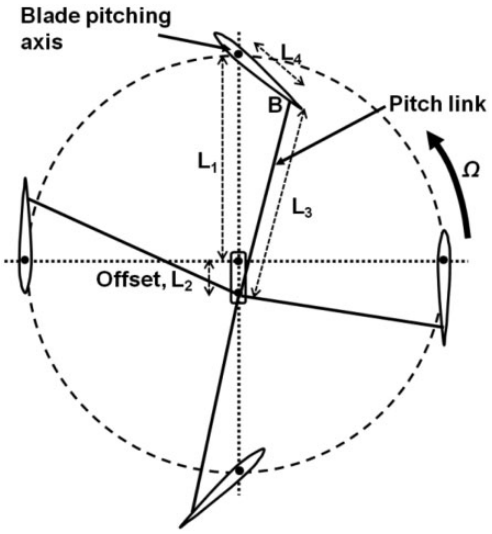


**Figure 14.** Pitching mechanism on the meso-scale cyclorotor.

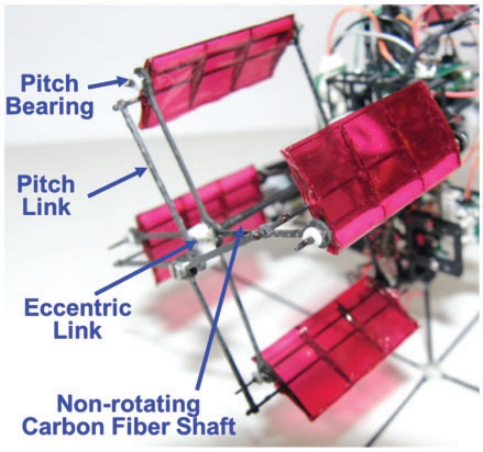


**Figure 15.** Pitching mechanism implemented on the cyclorotor.

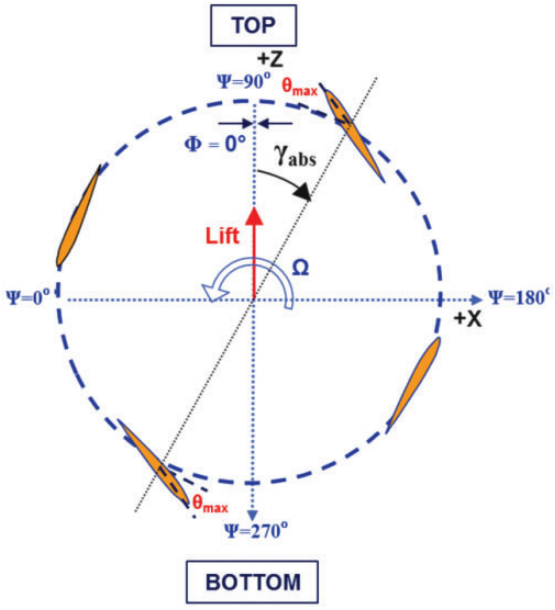


**Figure 16.** Cyclorotor coordinate system.

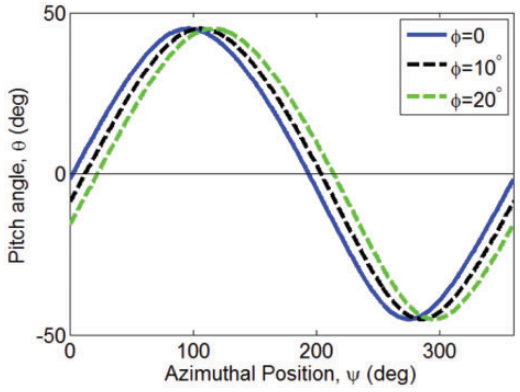


**Figure 17.** Blade pitch angle as a function of rotor azimuth for each cyclorotor at trim.

axis. The connections at both ends of the pitch link are through pin joints to allow the rotational degree of freedom. With this arrangement, as the rotor rotates, the blades automatically pitch cyclically. Because the pitching amplitude depends on the offset length, $L_2$, the offset length is kept at a constant value to achieve 45° pitching amplitude. The rotation of the offset link changes the phasing of the cyclic pitching and thereby changes the direction of the thrust vector.

Figure 15 shows the actual pitching mechanism implemented on the meso-scale cyclorotor. The current pitching mechanism requires the offset link ($L_2$) to be installed at the tip of shaft in a non-rotating frame. In order to reduce mechanical complexities, the distance $L_2$ is kept constant. With a fixed maximum blade pitching amplitude, the magnitude of thrust is modulated during flight by varying the rotational speed.

The direction of the thrust vector can be manipulated by rotating the offset link, which changes the phasing of the harmonic pitching schedule. For the current coordinate system (Figure 16), the azimuthal position of the blade ($\Phi$) is measured clockwise from the horizontal axis of rotation and is equivalent to zero when the blades are at the leftmost side of the circular trajectory. The time-varying aerodynamic forces produced by the cyclorotor can be resolved into the vertical and horizontal directions with a positive x-axis extending towards the right and a positive z-axis towards the top. In the figure, the phasing angle is denoted as $\gamma$, which is zero when aligned with the z-axis and positive with a clockwise rotation.

Even though they produce identical values of thrust at each r/min, the meso-scale cyclorotors have different pitch phasings in order to counteract the clockwise

reaction torque from the tail rotor (Figure 17). As a result, the cyclorotor on the right has a higher phasing which tilts the thrust vector forward and produces a net counterclockwise yaw moment of the vehicle. The thrust vectoring mechanism on the cyclocopter that is used to rotate the offset link and provide a phasing input is composed of two 1.5 g micro linear servo actuators that are connected to the pitching mechanism through linkages. The servos allow for $\pm 20^{\circ}$ of thrust vectoring.

### *Tail rotor*

The tail rotor used on the cyclocopter is optimized for high power loading through a previous study on micro-rotors.[21] The thin (t/c = 1.17%) 2-bladed carbon fiber rotor has $\sigma = 0.32$, circular cambered plate airfoil with a sharp leading edge, taper ratio of 0.5,−11.4° twist, and a camber of 6.1% at 75% span location. The blades are manufactured using carbon fiber prepreg and are attached together using a rapid prototyped plastic hub. Results of the previous study showed that the optimized rotor is able to achieve a maximum figure of merit (FM) of 0.67, which is significant for a rotor at the micro-scale. The tail rotor is able to provide up to 33 g of thrust at 8000 r/min, but the actual thrust is dictated by the pitch trim in hover (Figure 18). Flight testing data showed that the tail rotor actually operates at 5000 r/min and produces about 15 g to compensate for pitching moment from the cyclorotors.

## Onboard instrumentation

Without additional attitude stabilization through a closed-loop feedback system, the cyclocopter was found to be highly unstable due to limited inherent aerodynamic damping.[8] The control and flight dynamics were further complicated by the presence of strong gyroscopic roll–yaw coupling. Onboard attitude stabilization is implemented using ELKA, a custom embedded processor-sensor board developed for the twin-cyclocopter (Figure 19). The board weighs only 1.3 g and is powered by a single 1-cell 3.7 V 125 mAh Li-Po battery. ELKA houses a STM32 microprocessor with a 32-bit ARM Cortex M3 core for high-end onboard computation tasks. The MPU-9150 IMU integrated on the board includes tri-axial gyroscopes, accelerometers, and magnetometers. Wireless communications are serviced by an on-board nRF24L01 chip and a low-power 2.4 GHz RF transceiver. ELKA has a sensor update rate of 500 Hz and is capable of streaming vehicle attitude data and actuator controls data to the base station.

### *Telemetry*

The user communicates with the onboard controller using a LabVIEW interface through a wireless IEEE 802.15.4 data link (Figure 20). The board receives pilot inputs through a commercial Spectrum receiver which connects to the transmitter through a wireless 2.4 GHz radio link. A separate connection between the Spectrum receiver and transmitter ensures that the pilot will still have command over the vehicle if connection is lost between the ground station and the onboard processor. The ground station allows the user to modify the gains of the feedback system, sensitivity of pilot inputs, gyroscopic mixing ratios, and record attitude data transmitted by the onboard processor. All the data processing, feedback control calculations, and roll–yaw decoupling methods are performed onboard by ELKA.

## Controls strategy

Figure 21 shows the definition of pitch, roll, and yaw degrees of freedom for the twin-cyclocopter. As previously mentioned, both the cyclorotors rotate clockwise in the same direction such that there is a pitch-down moment that must be counteracted by a horizontal tail rotor, which is also used for pitch control. A stable and controlled hover requires a unique combination of

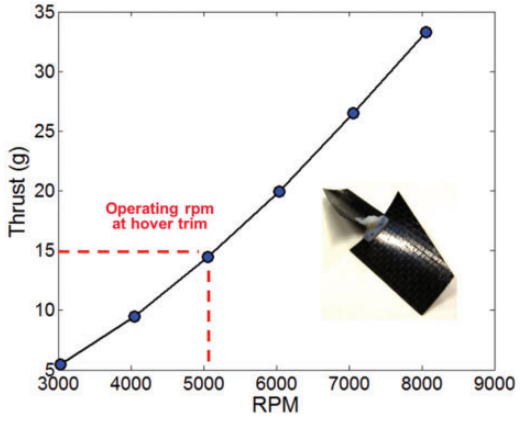


**Figure 18.** Thrust vs. r/min for tail rotor.

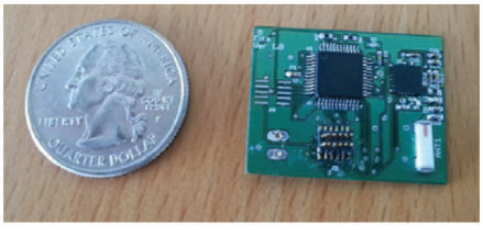

**Figure 19.** ELKA, 1.3 g processor-sensor board developed at UMD.

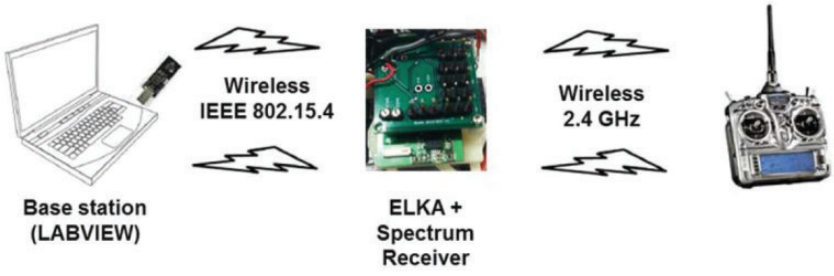


**Figure 20.** Wireless communication sequence on the cyclocopter.

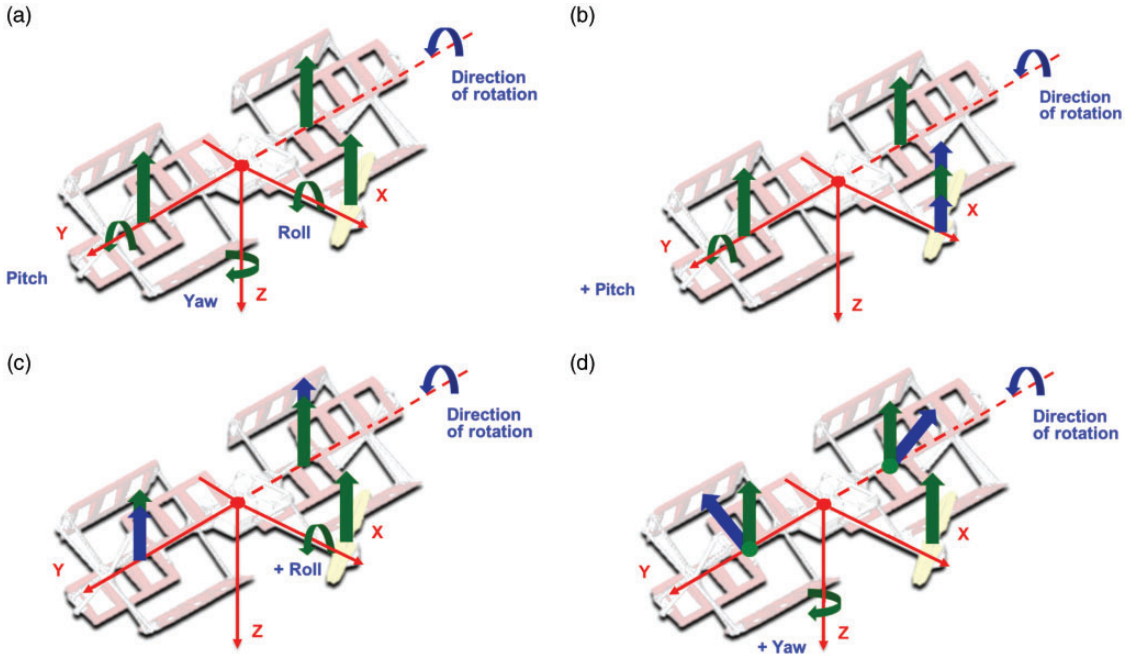


**Figure 21.** Control strategy for the twin-cyclocopter. (a) Definition of pitch, roll, and yaw degrees of freedom; (b) pitch control using tail rotor r/min; (c) roll control using differential r/min, and (d) yaw using thrust vectoring.

independent rotational speed of all three motors and thrust vectoring of the cyclorotors.

A positive roll is produced by increasing the r/min of the left rotor and decreasing the r/min of the right rotor. Finally, yaw is controlled through differential rotation/tilting of the two cyclorotor thrust vectors. The cyclorotors spin in the same direction along the + Y-axis so there is a net angular momentum that induces gyroscopic coupling between the roll and yaw degrees of freedom. To eliminate the gyroscopic coupling, an onboard control mixing was implemented where the roll and yaw inputs were appropriately combined to give decoupled motion.

## *Gyroscopic coupling*

Cyclocopter dynamics are dominated by gyroscopic cross-coupling caused by a net angular momentum from the cyclorotors spinning in the same direction. For a positive roll input, the vehicle responds in both roll right and counterclockwise yaw (Figure 22). Likewise, for a positive yaw input, the vehicle responds in clockwise yaw and also rolls to the right.

Instead of accounting for this effect through mechanical means, the cross-coupling is decoupled by mixing roll and yaw inputs in the controller. For example, to achieve a pure roll right response, a roll right input is combined with a clockwise yaw input to cancel out the inherent cross-coupling response. Likewise, for clockwise yaw, the input is appropriately combined with a roll left input. The mixing ratio is only applied to the open-loop pilot input and directly implemented on the onboard controller.

To find the appropriate gyroscopic mixing terms, the cyclocopter was suspended about c.g. on a 3-DOF gimbal stand that enables pitch, roll, and yaw motions.

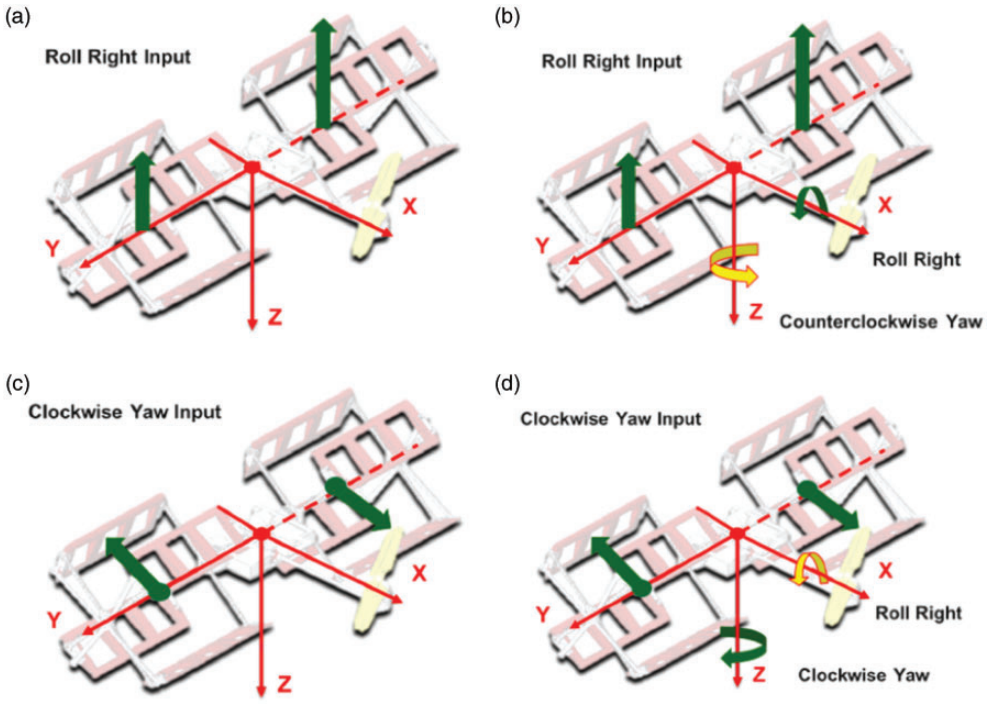


**Figure 22.** Gyroscopic cross-coupling between roll and yaw degrees of freedom. (a) Roll right control input, (b) roll-yaw response, (c) yaw control input, and (d) yaw-roll response.

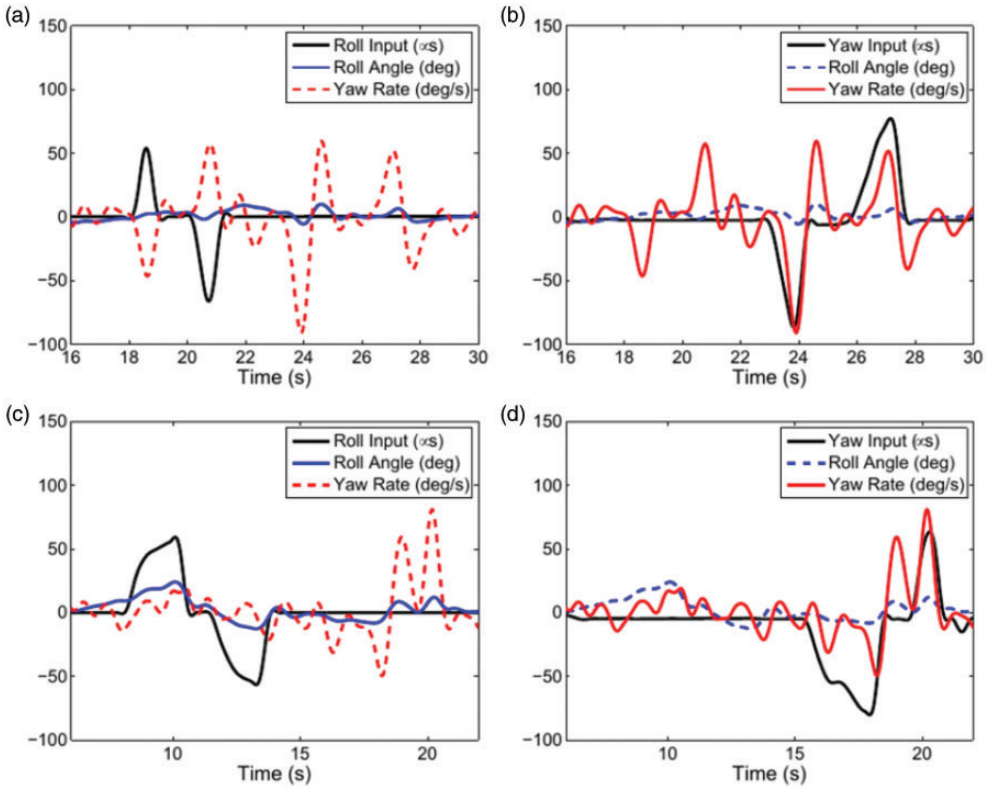


**Figure 23.** Response of vehicle before (a, b) and after (c, d) implementing gyroscopic mixing.

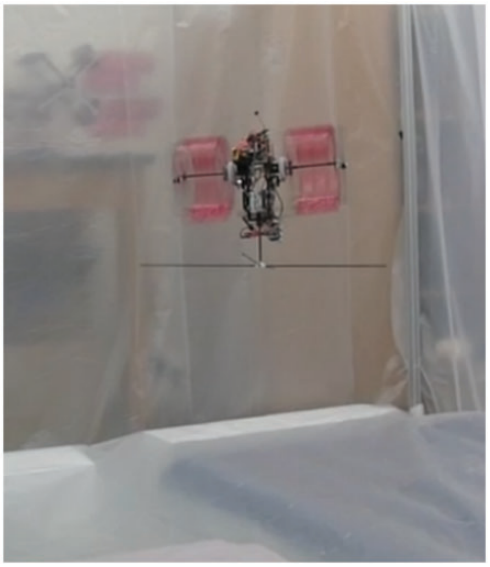

**Figure 24.** Stable sustained hover.

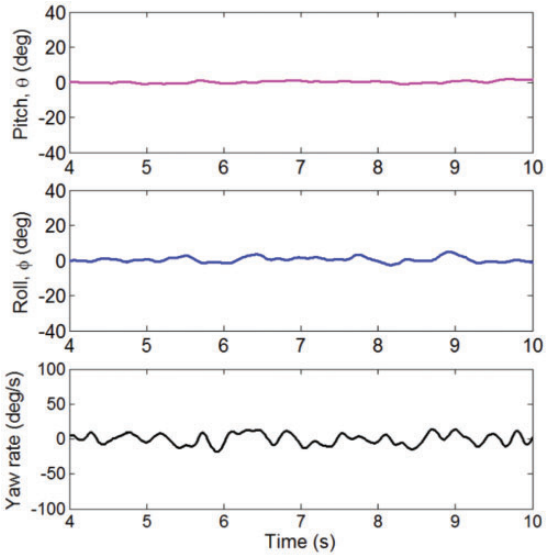


**Figure 25.** Pitch, roll, and yaw states for frimmed hover.

Starting with zero mixing, the constants for both roll and yaw inputs were slowly increased until the vehicle achieved a decoupled response. Experimental results showed a stronger coupling for a roll input, which results in higher mixing ratios. One reason for a stronger roll–yaw coupling could be that the moment of inertia about the x-axis is greater than that about the z-axis. The attitude data captured by ELKA (Figure 23) shows that the mixing ratio is able to sufficiently decouple the gyroscopic roll–yaw coupling. The next section describes the implementation of closed-loop feedback control for attitude stabilization.

## Closed-loop feedback control

Onboard closed-loop feedback is implemented using proportional-derivative (PD) control. This framework has been flight-proven for previous twin-cyclocopters in various flight conditions and is used on the meso-scale cyclocopter. The feedback states are aircraft pitch and roll Euler angles ($\phi$, $\theta$) and the attitude rates (p, q and r). An outer loop for vehicle positioning is serviced by a remote pilot. The final control inputs to the vehicle actuators are the individual rotational speeds of the rotors and the two servo inputs.

The pitch (q), roll (p), and yaw (r) attitude rates reported by the tri-axial gyroscopes are combined with the data provided by the accelerometer using a complementary filter to refine attitude measurements. The integration of gyro measurements with time has been known to cause drift in attitude estimation.[22] To account for the drift, a high pass complementary filter is used with a 4 Hz cut-off frequency for the gyro measurements. Vibrations from the rotary systems affected accelerometer measurements, which are processed through a low pass complementary filter with a 6 Hz cut-off frequency to reject disturbances from the rotor vibrations occurring at significantly higher frequencies than the body dynamics.

## Flight test results

During the flight tests, the proportional and derivative gains were tuned using the Ziegler Nichols approach. The gains that offered acceptable stiffness and damping to reject external disturbance with minimal oscillations were chosen. While the form of the control strategy is fixed, the gains and control inputs for trimmed flight were higher than the ones obtained through gimbal testing because the setup provided artificial damping in pitch, roll, and yaw due to friction from the bearing. In addition, the gimbal was slightly misaligned from the vehicle's true center of gravity.

Flight tests were systematically conducted by first providing a pure throttle command and observing the vehicle response. Any forward translation was counteracted by either uniformly reducing the phasing of the cyclic blade pitch or varying the tail propeller r/min. After fine-tuning the gains, the present vehicle successfully demonstrated stable hover (Figure 24). Onboard attitude data show satisfactory attitude angles and rates (Figure 25). The results show that the empty weight fraction of the cyclocopter can be feasibly reduced to develop a lightweight and versatile cyclocopter.

## Conclusion

The objective of this research was to demonstrate the cyclocopter's potential to be a robust light-weight

MAV platform by developing a 60 g meso-scale twin-cyclocopter capable of stable, sustained hover. One of the biggest challenges is that the cyclorotors comprise a significant portion (23–34%) of the empty weight fraction of the vehicle. The key to reducing cyclorotor weight is by designing lightweight blades with high bending and torsional stiffness. Another challenge is that cyclocopter dynamics are dominated by gyroscopic cross-coupling caused by a net angular momentum from the cyclorotors spinning in the same direction. To eliminate the cross-coupling, a mixing strategy was implemented with the onboard controller. The following is the summary and some of the specific conclusions drawn from this study:

1. The 60g meso-scale twin-cyclocopter successfully demonstrated stable, sustained hover. Since both the cyclorotors rotate clockwise in the same direction, there is a pitch-down moment that must be counteracted by a horizontal tail rotor. Anti-torque capability from the tail rotor is augmented by increasing the horizontal offset between this rotor and vehicle's center of gravity. The offset reduces the thrust required from the tail rotor and minimizes the rotor size.
2. Major reductions in vehicle weight were possible due to aerodynamically and structurally optimized lightweight cyclorotor using an innovative blade design. The new blade design is a composite structure with a foam leading edge and carbon fiber ribs, spars, and stringers. The NACA 0015 ribs are milled out of carbon fiber and are evenly distributed along the span to maintain the airfoil shape. The pitching axis is provided by a carbon fiber spar that runs through the entire blade structure and an additional carbon fiber spar provides a connection to the blade pitching mechanism. The new blade design is also 67% lighter than the conventional blade design.
3. Key parameters in cyclorotor performance are blade structure, blade geometry, rotor geometry, and blade kinematics. Based on the results of the parametric study conducted in this research, the optimized cyclorotor on the 60 g twin-cyclocopter utilizes four 0.50 g blades with the new blade design, c/R ratio of 0.57, and pitching axis location at 25% of blade chord. Along with other structural components, the optimized cyclorotor weighs 7 g and has a thrust-to-weight (T/W) ratio of approximately 3 at the operating rotational speed of 3000 r/min (T = 23 g).
4. Gyroscopic effect dominates cyclocopter dynamics because of the unbalanced angular momentum that is twice in magnitude from the two cyclorotors spinning in the same direction. For a positive roll input, the vehicle responds in both roll right and counterclockwise yaw. Likewise, for a positive yaw input, the vehicle responds in clockwise yaw and also rolls to the right.
5. The cross-coupling is decoupled by mixing roll and yaw inputs in the controller. To achieve a pure roll right response, a roll right input is combined with a clockwise yaw input to cancel out the inherent cross-coupling response. Likewise, for clockwise yaw, the input is appropriately combined with a roll left input. The mixing ratio is only applied to the open-loop pilot input and directly implemented on the onboard controller.
6. The cyclocopter is inherently unstable and requires an inner-loop attitude stabilization. With a take-off mass of 60 g, it is particularly challenging for this vehicle to achieve stability because of lower inertia and faster vehicle dynamics compared to cyclocopters at larger scales. A proportional-derivative controller for the feedback controls system can sufficiently stabilize the vehicle. ELKA, an ultra-light (1.3 g) onboard processor-sensor board was successfully developed for the cyclocopter and is able to update the inner-loop attitude stabilization at 500 Hz.

## Acknowledgements

The authors would like to thank Dr. Vikram Hrishikeshavan for his inputs on the controls system and troubleshooting with any problems associated with ELKA. They also thank Jerry Andrews and Victoria Martin for their assistance with vehicle construction and testing.

## Declaration of conflicting interests

The author(s) declared no potential conflicts of interest with respect to the research, authorship, and/or publication of this article.

## Funding

The author(s) disclosed receipt of the following financial support for the research, authorship, and/or publication of this article: This research was supported by the Army's MAST CTA Center for Microsystem Mechanics with Dr. Brett Piekarski (ARL) and Mr. Chris Kroninger (ARL-VTD) as Technical Monitors.

## References

1. McMichael JM and Francis CMS. Micro air vehicles: toward a new dimension in flight. U.S Department of Defense Weaponse Systems Technology Information Analysis Center (WSTIAC) Newsletter, vol. 1, No. 1–3, Jan–Jul 20.
2. Pines D and Bohorquez F. Challenges facing future micro-air-vehicle development. *J Aircraft* 2006; 43: 290–305.
3. Leishman JG. *Principles of helicopter aerodynamics*. New York, NY: Cambridge University Press, 2000.

4. Benedict M, Ramasamy M, Chopra I, et al. Performance of a cycloidal rotor concept for micro air vehicle applications. *J Am Helicop Soc* 2010; 55: 022002-1–022002-14.
5. Benedict M, Ramasamy M and Chopra I. Improving the aerodynamic performance of micro-air-vehicle-scale cycloidal rotor: an experimental approach. *J Aircraft* 2010; 47: 1117–1125.
6. Benedict M, Jarugumilli T, Lakshminarayan VK, et al. Experimental and computational studies to understand the role of flow curvature effects on the aerodynamic performance of a MAV-scale cycloidal rotor in forward flight. In: *Proceedings of the 53rd AIAA/ASME/ASCE/AHS/ASC structures, structural dynamics, and materials conference*, Honolulu, Hawaii, 23–26 April 2012.
7. Jarugumilli T, Benedict M and Chopra I. Experimental investigation of the forward flight performance of a MAV-scale cycloidal rotor. In: *Proceedings of the 68th annual national forum of the American Helicopter Society*, Fort Worth, TX, 13 May 2012.
8. Hrishikeshavan V, Benedict M and Chopra I. Flight dynamics identification of a cyclocopter micro air vehicle in hover. In: *Proceedings of the 69th annual national forum of the American Helicopter Society*, Phoenix, Arizona, 21–23 May 2012.
9. Benedict M, Shrestha E, Hrishikeshavan V, et al. Development of 200 gram twin-rotor micro cyclocopter capable of autonomous hover. In: *Proceedings of the American Helicopter Society future vertical lift aircraft design conference*, San Francisco, CA, 18–20 January 2012.
10. Shrestha E, Benedict M, Hrishikeshavan V, et al. Development of a 100 gram micro cyclocopter capable of autonomous hover. In: *Proceedings of the 38th European rotorcraft forum*, Amsterdam, Netherlands, 4–7 September 2012.
11. Benedict M, Gupta R and Chopra I. Design, development, and open-loop flight testing of a twin-rotor cyclocopter micro air vehicle. *J Am Helicop Soc* 2013; 58: 1–10.
12. Shrestha E, Hrishikeshavan V, Benedict M, et al. Development of control strategies and flight testing of a twin-cyclocopter in forward flight. In: *Proceedings of the 70th annual national forum of the American Helicopter Society*, Montreal, Quebec, Canada, 20–22 May 2014.
13. Harrington A and Kroninger C. Characterization of small DC brushed and brushless motors. Army Research Laboratory no. ARL-TR-6389, March 2013.
14. Benedict M, Jarugumilli T and Chopra I. Effect of rotor geometry and blade kinematics on cycloidal rotor hover performance. *J Aircraft* 2013; 50: 1340–1352.
15. Benedict M. *Fundamental understanding of the cycloidal-rotor concept for micro air vehicle applications*. PhD Thesis, Department of Aerospace Engineering, University of Maryland College Park, 2010.
16. Benedict M, Jarugumilli T and Chopra I. Experimental performance optimization of a MAV-scale cycloidal rotor. In: *Proceedings of the AHS specialists' meeting on aeromechanics*, San Francisco, CA, 20–22 January 2010.
17. Benedict M, Mattaboni M, Chopra I, et al. Aeroelastic analysis of a MAV-scale cycloidal rotor. In: *Proceedings of the 51st AIAA/ASME/ASCE/AHS/ASC structures, structural dynamics, and materials conference*, Orlando, FL, 12–15 April 2010.
18. Benedict M, Ramasamy M, Chopra I, et al. Performance of a cycloidal rotor concept for micro air vehicle applications. *J Am Helicop Soc* 2010; 55: 022002-1–022002-14.
19. Migliore PG, Wolfe WP and Fanuccif JB. Flow curvature effects on darrieus turbine blade aerodynamics. *J Energy* 1980; 4: 49–55.
20. Benedict M. *Fundamental understanding of the cycloidal-rotor concept for micro air vehicle applications*. PhD Thesis, Department of Aerospace Engineering, University of Maryland College Park, 2010.
21. Benedict M, Winslow J, Hasnain Z, et al. Performance and flowfield measurements of a MAV-scale helicopter rotor in hover. In: *Proceedings of the 70th annual national forum of the American Helicopter Society*, Montreal, Canada, 20–22 May 2014.
22. Thong YK, Woolfson MS, Crowe JA, et al. Dependence of inertial measurements of distance on accelerometer noise. *Meas Sci Technol* 2002; 13: 1163–1172.